Histol Histopathol (2020) 35: 811-825

http://www.hh.um.es

Histology and Histopathology
From Cell Biology to Tissue Engineering

Spatial and phenotypic characterization of pancreatic cancer-associated fibroblasts after neoadjuvant treatment

Michael Friberg Bruun Nielsen[1,2,3], Michael Bau Mortensen[2,3,4], Mia Dahl Sørensen[1,3], Martin Wirenfeldt[1,3], Bjarne Winther Kristensen[1,3], Henrik Daa Schrøder[1,3], Per Pfeiffer[2,3,5] and Sönke Detlefsen[1,2,3]

[1]Department of Pathology, [2]Odense Pancreas Center (OPAC), Odense University Hospital, [3]Department of Clinical Research, Faculty of Health Sciences, University of Southern Denmark, [4]Department of Surgery, HPB Section and [5]Department of Oncology, Odense University Hospital, Odense, Denmark

Summary. Pancreatic ductal adenocarcinoma (PC) is characterized by a highly fibrotic desmoplastic stroma. Subtypes of cancer-associated fibroblasts (CAFs) have been identified in chemotherapy-naïve PC (CTN-PC), but their precise functions are still unclear. Our knowledge regarding the properties of CAFs in the regressive stroma after neoadjuvant treatment (NAT) of PC (NAT-PC) is particularly limited. We aimed to examine the marker phenotypic properties of CAFs in the regressive stroma of PC.

Surgical specimens from patients with CTN-PC (n=10) and NAT-PC (n=10) were included. Juxtatumoural, peripheral, lobular, septal, peripancreatic, and regressive stromal compartments were manually outlined using digital imaging analysis (DIA) for area quantification. The compartment-specific expression of CD271, cytoglobin, DOG-1, miR-21, osteonectin, PDGF-Rβ, and tenascin C was evaluated by immunohistochemistry or *in situ* hybridization, using manual scoring and automated DIA.

The area fraction of the regressive stroma was significantly higher in NAT-PC than in CTN-PC (P=0.0002). CD271 (P<0.01), cytoglobin (P<0.05), DOG1 (P<0.05), miR-21 (P<0.05), and tenascin C (P<0.05) exhibited significant differences in their expression profiles between the juxtatumoural compared to the peripheral and regressive stroma. PDGF-Rβ expression was significantly higher in juxtatumoural than in peripheral CAFs (P<0.05).

Our data provide further support of the concept of stromal heterogeneity and phenotypic different CAF subtypes in PC. CAFs in the regressive stroma of NAT-PC show a marker phenotype similar to some (namely, peripheral) and different from other (namely, juxtatumoural) previously defined CAF subtypes. It may be hypothesized that phenotypic CAF subtypes, at least in part, also may share functional properties. Studies examining the precise functional characteristics of CAF subtypes in PC are needed.

Key words: Pancreatic cancer, Neoadjuvant treatment, FOLFIRINOX, Tumour stroma, Cancer-associated fibroblasts

Offprint requests to: Sönke Detlefsen, J.B. Winsløws Vej 15, 5000 Odense C, Denmark. e-mail: Sonke.Detlefsen@rsyd.dk

DOI: 10.14670/HH-18-201

Introduction

Pancreatic ductal adenocarcinoma (PC) has a dismal prognosis, with data from Danish patients indicating an overall 5-year survival rate of 5% and a median survival time of only 5.9 months (DPCD, 2017). PC is characterized by a prominent desmoplastic stroma produced by cancer-associated fibroblasts (CAFs) (Yen et al., 2002; Erkan et al., 2008; Farrow et al., 2009; Nielsen et al., 2016). Fibrosis is a hallmark of PC visible by microscopy, and the fibrotic stroma can occupy up to 80% of the total tumour volume (Kadaba et al., 2013). However, the exact role of the desmoplastic stroma and CAFs in PC progression has not been fully elucidated (Gore and Korc, 2014).

The most important precursor cells for CAFs in PC are quiescent pancreatic stellate cells (qPSCs) (Apte et al., 1998; Bachem et al., 1998; Erkan et al., 2012). It has previously been demonstrated that qPSCs express cytoglobin and that the expression of this marker is sustained upon activation in CAFs (Nielsen et al., 2017; 2018). Previous studies indicate that spatially and phenotypically distinct subtypes of CAFs exist in PC (Iacobuzio-Donahue et al., 2002; Sugimoto et al., 2006; Öhlund et al., 2017; Haeberle et al., 2018; Nielsen et al., 2018). Juxtatumoral/perilesional CAFs are located in close vicinity to the PC cells, while the peripheral CAFs are found at a greater distance from them (Iacobuzio-Donahue et al., 2002; Öhlund et al., 2017; Haeberle et al.; 2018, Nielsen et al., 2018). It was reported that the marker phenotype of juxtatumoural CAFs is characterized by high expression of CD10, cytoglobin, discovered on gastrointestinal stromal tumours 1 (DOG1), MMP11, Apolipoprotein C-1, Apolipoprotein D, and miR-21 and by low expression of CD271 (Iacobuzio-Donahue et al., 2002; Nielsen et al., 2018). Furthermore, peripheral CAFs display the opposite antigen expression, with high expression of CD271 and limited expression of CD10, cytoglobin, DOG1, and miR-21 (Nielsen et al., 2018). Tenascin C is predominantly expressed in the juxtatumoural extracellular matrix (ECM) compared to the peripheral ECM in PC (Nielsen et al., 2018). Several prognostic studies show that juxtatumoural CAF markers, such as CD10 and miR-21, hold negative prognostic value in PC, while high stromal expression of CD271 is associated with a better prognosis (Dang et al., 2006; Ikenaga et al., 2010; Fujiwara et al., 2012; Kadera et al., 2013). Overall, the functional role of CAF subtypes in PC has not been elucidated. However, it is tempting to speculate whether these data may indicate that (some of the) juxtatumoural CAFs and the juxtatumoural stroma may play a more growth-promoting role in PC progression than (some of the) peripheral CAFs and the peripheral stroma (Iacobuzio-Donahue et al., 2002; Nielsen et al., 2018).

It is generally accepted that "regressive fibrosis" is a hallmark of the histological response to neoadjuvant treatment (NAT) with FOLFIRINOX in PC (Chatterjee et al., 2013; Verbeke et al., 2015; Pai and Pai, 2018). However, the marker phenotypic properties of fibroblasts in regressive fibrosis (regressive CAFs) are currently unknown. Several studies have described histological responses, such as clusters of multinucleated foreign body-type giant cells, cholesterol clefts, fibrosis and repair reactions, to FOLFIRINOX treatment in PC, but the antigen expression of fibroblasts located in this regressive type of stroma has, to the best of our knowledge, not been elucidated (Jones et al., 2013; Gostimir et al., 2016; Haeberle et al., 2017). Haeberle et al. tested whether biomarkers are useful for the differentiation of tumour regression from tumour desmoplasia, but concluded that this distinction remains challenging when based on single markers (Haeberle et al., 2017).

In this study, we aimed to examine the marker phenotype of CAFs in the regressive stroma of NAT-PC, with special emphasis on similarities or dissimilarities with juxtatumoural and peripheral CAFs. We defined six stromal compartments in resection specimens with PC: the juxtatumoural, peripheral, regressive, lobular, septal, and peripancreatic stroma. The compartment-specific expression of CD271, cytoglobin, DOG1, miR-21,

Table 1. Patient and tumour characteristics in 10 neoadjuvantly treated pancreatic cancer patients (NAT-PC) and 10 chemotherapy-naïve pancreatic cancer patients (CTN-PC).

Characteristics		CTN-PC	NAT-PC
Number	n	10	10
Age	Mean, years (range)	69.9 (52.8-79.8)	61.6 (49.8-75.9)
Sex	Female/male	6/4	5/5
Neoadjuvant treatment with FOLFIRINOX	n	0	10
Time from completion of neoadjuvant treatment until tissue retrieval	Mean, days (range)	-	33.8 (14-68)
Tumour differentiation grade	G1/G2/G3	2/7/1	1/8/1
pT stage[#]	T1/T2/T3/T4	1/0/9/0	2/0/8/0
pN stage[#]	N0/N1	0/10	5/5
Surgical procedure			
Whipple resection	n	10	10
Survival data			
Patients alive at time of analysis	n	5	5
Observational time for patients alive	Mean, months (range)	34.9 (16.2 – 55.5)	35.1 (25.1-48.5)
Median survival	Median, months (SE)	32.2 (6.4)	40.4 (7.3)

[#]: According to the UICC pathological Tumour-Node-Metastasis (pTNM) classification version 7 (Sobin et al., 2009). FOLFIRINOX: Folinic acid, Fluorouracil, Irinotecan, Oxaliplatin, NAT-PC: neoadjuvantly treated pancreatic cancer, CTN-PC: chemotherapy-naïve pancreatic cancer, SE: standard error.

osteonectin (SPARC), platelet-derived growth factor receptor β (PDGF-Rβ), and tenascin C was evaluated semiquantitatively and using automated digital image analysis (DIA) in PC tissues from patients who had received NAT (NAT-PC) and from patients who were chemotherapy-naïve (CTN-PC), using immunohistochemistry (IHC) and *in situ* hybridization (ISH).

Materials and methods

Tissue specimens

Ten CTN-PC patients and 10 NAT-PC patients treated with FOLFIRINOX (Folinic acid, Fluorouracil, Irinotecan, and Oxaliplatin) prior to surgery for the purpose of downstaging were included in this study (Table 1). From each surgical specimen, one formalin-fixed paraffin-embedded (FFPE) tissue block was included.

The database of the Department of Pathology, Odense University Hospital, was searched for pancreatic surgical specimens that were obtained beginning on January 1, 2015, and thereafter. All included cases were re-examined by a pancreatic pathologist, and only pancreatic ductal adenocarcinomas (PDACs) were included in the study. Tumours originating from an intraductal papillary mucinous neoplasm (IPMN); originating from the ampulla of Vater, distal common bile duct or duodenum; and secondarily involving the pancreas were excluded. In this report, we use the term PC to indicate PDAC throughout. The FFPE tissue block that was most representative for each case was selected. Regarding the CTN-PC specimens, special emphasis was on the histologic grade (G2) and growth pattern. Regarding the NAT-PC specimens, special emphasis was on the presence of regressive features, such as regressive fibrosis, hyalinosis, acellular mucin lakes, and accumulation of macrophages.

This study was approved by the Ethics Committee of the Region of Southern Denmark (project-ID: S-20140168) and the Danish Data Protection Agency (project-ID: 15/33101). We ensured that patients had not advocated against the use of their tissue in the Danish registry for the use of tissue in research ('Vævsanvendelsesregisteret').

Immunohistochemistry (IHC)

Four-micron-thick sections were cut on a microtome and mounted on FLEX IHC slides (Dako, Glostrup, Denmark). The IHC staining procedures for some antigens were automated, and some antigens were stained manually. Heat-induced epitope retrieval (HIER) and non-HIER protocols were tested for antigen retrieval to obtain the highest signal-to-noise ratio. Details regarding antibody specifications, dilutions, incubation times, and epitope retrieval procedures for each antigen are presented in Table 2.

Manual IHC staining procedures were used for cytoglobin and PDGF-Rβ. Tissue sections were dewaxed with xylene and rehydrated with an ethanol gradient in water. Incubation in 1.5% H_2O_2 (Merck, Darmstadt, Germany) was performed to block endogenous peroxidase activity. Tissue sections were placed in HIER buffer and exposed to three successive steps using a microwave oven (NN-SD450W, Panasonic, Osaka, Japan): (1) 9 min at 900 W, (2) 15 min at 440 W, and (3) 15 min at room temperature (RT). Nonspecific binding was blocked by incubation for 30 min in 2% BSA. The sections were incubated with primary antibody diluted in antibody diluent S2022 (Dako, Glostrup, Denmark) for 60 min at RT or overnight at 4°C. Unbound primary antibodies were washed away, and the EnVision+ peroxidase/DAB detection system (Dako, Glostrup,

Table 2. List of antibodies, retrieval methods, incubation times, dilutions and staining platforms used for immunohistochemistry.

Antigen	Species and clonality	Company	Clone/ Product ID	Epitope retrieval	Incubation	Dilution	Platform	Detection
α-SMA	Mouse, mAb	Nordic BioSite	BS66	HIER: CC1_32_100	16min / 36°C	1:1000	BenchMark	OptiView
Caldesmon	Mouse, mAb	Dako	M3557	Non-HIER: Protease 3/4 + HIER: CC1_32_100	16min / 36°C	1:100	BenchMark	OptiView
CD163	Mouse, mAb	Ventana Medical Systems	MRQ-26	HIER: CC1_32_100	32min / 36°C	RTU	BenchMark	OptiView
CD271	Mouse, mAb	Cell Marque	MRQ-21	HIER: TRS_30_97	20min / 32°C	1:2000	Omnis	EnVision
Cytoglobin	Rabbit, pAb	Sigma Aldrich	HPA017757	HIER: EDTA / MWO 15min	O/N / 4°C	1:100	Manuel	EnVision
DOG1	Rabbit, mAb	Ventana Medical Systems	SP31	HIER: CC1_32_95 + Non-HIER: Protease (3/4)	8min / 36°C	RTU	BenchMark	OptiView
ERG	Rabbit, mAb	Ventana Medical Systems	EPR3864	HIER: CC1_32_100	16min / 36°C	RTU	BenchMark	OptiView
Maspin	Mouse mAb	Pharmingen	G167-70	HIER: CC1_32_100	32min / 36°C	1:100	BenchMark	OptiView
Osteonectin	Mouse, mAb	NovoCastra	15G12	HIER: CC1_48_100	16min / 36°C	1:200	BenchMark	OptiView
PDGF-Rβ	Rabbit, mAb	Cell Signaling	28E1	HIER: EDTA / MWO 15min	60min / RT	1:100	Manuel	EnVision
Tenascin C	Mouse, mAb	NovoCastra	49	HIER: CC1_32_95 + Non-HIER: Protease (3/4)	32min / 36°C	1:100	BenchMark	OptiView

α-SMA: α-smooth muscle actin, CC1: cell conditioning solution 1 (pH 8.5, Ventana Medical Systems), CC1_X_X: CC1_minutes incubated_degrees Celsius, CD: cluster of differentiation, DOG1: discovered on gastrointestinal stromal tumour 1, EDTA: ethylenediaminetetraacetic acid, ERG: ETS-related gene, HIER: heat-induced epitope retrieval, mAb: monoclonal antibody, MWO: microwave oven, O/N: overnight, pAb: polyclonal antibody, PDGF-Rβ: platelet-derived growth factor receptor β, Protease (X/X): Protease (variant/minutes incubated), RTU: ready to use, RT: room temperature.

Denmark) was used for detection of antigen-bound antibodies. Nuclear counterstaining was performed with Mayer's haematoxylin (Fagron Nordic, Copenhagen, Denmark). Slides were washed, dried and mounted with coverslips using Pertex (Histolab, Gothenburg, Sweden).

Automated protocols were used for α-smooth muscle actin (α-SMA), caldesmon, CD163, CD271, DOG1, ETS-related gene (ERG), maspin, osteonectin (SPARC), and tenascin C. The staining, including deparaffinization, epitope retrieval and blocking of endogenous peroxidase activity, was performed using either a BenchMark Ultra Immunostainer (Ventana Medical Systems, Tucson, AZ) with the OptiView Detection Kit (Ventana Medical Systems, Tucson, AZ) or a Dako Omnis instrument (Agilent, Santa Clara, US) with the Dako EnVision FLEX visualization system (Agilent, Santa Clara, US).

In situ hybridization

The probe sequences for miR-21, miR-126 (positive control, endothelial marker), and scramble (negative control) are listed in Table 3. The listed probes were all double-labelled with digoxigenin (DIG), and ISH was generally performed on 5-μm-thick paraffin sections as described elsewhere (Nielsen et al., 2011, 2018). The ISH analyses were performed in collaboration with Boye Schnack Nielsen, Bioneer A/S, Hørsholm, Denmark. Briefly, DIG-labelled locked nucleic acid (LNA) probes were detected with alkaline phosphatase-conjugated anti-DIG antibodies followed by incubation with 4-nitro-blue tetrazolium and 5-bromo-4-chloro-30-indolylphosphate as the substrate. All slides were counterstained with nuclear fast red, dehydrated and mounted using Entellan mounting medium (Fisher Scientific). miR-126 was positively expressed in endothelial cells in all examined tissue specimens, which indicate that the included tissue specimens were suitable for *ISH* analyses.

Sirius red

The procedures for the sectioning, mounting and deparaffinization steps were similar to those performed for the IHC analyses. Deparaffinized sections were first stained in Weigert's iron haematoxylin (15 min, Fagron Nordic). Following a washing step, the sections were stained with 0.1% Sirius Red (Ampliqon, Odense, Denmark) in picric acid (15 min, VWR, Søborg, Denmark). The slides were dehydrated and mounted with coverslips using Pertex.

Definition of stromal compartments in pancreatic resection specimens with PC and NAT-PC

We used a slightly modified and extended definition of the stromal compartments in pancreatic resection specimens with PC that we used in a previous study (Nielsen et al., 2018). This definition comprises six compartments, and takes also compartments that are characteristic of PC after NAT into account: The juxtatumoural, peripheral, lobular, septal, peripancreatic, and regressive stroma (Fig. 1) (Nielsen et al., 2018). It has to be emphasized that the juxtatumoural and peripheral compartments were considered an essential part of the malignant tumour, while the lobular, septal, and peripancreatic compartments were considered part of an inflammatory process in the vicinity of the tumour ("peritumoural pancreatitis").

The 1) juxtatumoural stroma was defined as the stroma located between 0 and 50 μm from the cancer cells (Fig. 1). The 2) peripheral stroma fulfilled the following criteria: It was 50-500 μm away from cancer cells, it was not inside lobuli, it was not inside septa, and it was not related to peripancreatic (fat tissue necrosis-associated) stroma. The stroma in the peritumoural pancreatic tissue was divided into lobular and septal stroma: The 3) lobular stroma was defined as the stroma located in intralobular areas, no further than 200 μm away from acinar cells, intralobular ducts and/or islets. The 4) septal stroma was defined as the stroma located in perilobular (septal) areas surrounding the pancreatic lobuli (Fig. 1). The width of the septa was defined as up to half the maximum diameter of the accompanying lobule. The 5) peripancreatic stroma was defined as the border between the pancreatic parenchyma and peripancreatic fat and contained fat cells, blood vessels, nerves, inflammatory cells, fibroblasts and ECM. Importantly, the peripancreatic stroma had to be devoid of acinar cells, islets of Langerhans, and ducts – if these structures were present, the stroma was considered to be lobular stroma. The 6) regressive stroma was defined as the stroma >500 μm away from cancer cells and had to be devoid of acinar cells, intralobular ducts, islets, and fat cells - if these structures were present, the stroma was considered to be lobular stroma. When cancer cells were

Table 3. List of LNA probes and experimental conditions used for *in situ* hybridization analyses.

Target RNA	nt	Probe sequence	T_m (°C)	T_{hyb} (°C)	Probe concentration (nM)
miR-21-5p	22	TCAACATCAGTCTGATAAGCTA	83	60	2
miR-126-3p	20	CATTATTACTCACGGTACGA	84	60	10
Scramble	21	TGTAACACGTCTATACGCCCA	87	60	10

nt: nucleotides, T_{hyb}: hybridization temperature, T_m: predicted probe: RNA melting temperature.

present within the lobular, septal, peripancreatic or regressive stroma, the juxtatumoural and peripheral compartments were defined as described above also at these sites.

Blinded manual microscopic evaluation of pancreatic resection specimens with NAT-PC and CTN-PC

A board-certified pathologist (MW) examined the H&E-stained slides of the ten NAT-PC and ten CTN-PC specimens without any prior information on the treatment history of the patients. The histological response was evaluated using a slightly modified CAP (College of American Pathologists) tumour regression grading (TRG) system (Washington et al., 2013). We used a system allowing for a more detailed evaluation of histological regression, consisting of 5 different grades of regression (0 to 4), while the original CAP TRG system was based on 4 different grades (0 to 3). TRG score 0 indicated a complete response, with no residual cancer (only regressive features); TRG score 1 indicated a near-complete response, with minimal residual cancer cells; TRG score 2 indicated a major response, with more regressive features than cancer cells; TRG score 3 indicated a minimal response, with more cancer cells than regressive fibrosis; and TRG score 4 indicated no response, characterized by a lack of any regressive features. Notably, regressive features, such as regressive fibrosis, hyalinosis, acellular mucin lakes, and the accumulation of macrophages could sometimes be observed focally in CTN-PC, possibly due to an inflammatory or immunological host-versus-tumour response.

Quantification of stromal compartments

Area quantification of the stromal compartments was performed with the VIS Image Analysis Software, version 2018.4 (Visiopharm, Hørsholm, Denmark). Digitalized (40x objective) H&E-stained slides of the ten NAT-PC specimens and ten CTN-PC specimens were imported to the program for subsequent analysis. According to the definitions above, the six compartments were manually outlined and defined as regions of interest (ROIs) (Fig. 1). In addition, areas with tumour cells, ductal structural collagen, periductal inflammation, and dysplastic cells/PanINs were outlined and defined as individual ROIs (Fig. 2A,B). The area of each ROI was determined by the VIS Image Analysis Software. All remaining structures (excluded regions), including fat, blood vessels, nerves, duodenum, lymph nodes, and the common bile duct, were combined into and outlined as one region but were not included in the total ROI area. The regressive stroma fraction (RS) was calculated by dividing the area of regressive stroma by the sum of the area of the juxtatumoural, peripheral and regressive stroma, multiplied by 100.

Evaluation of interobserver variability for identification and quantification of stromal compartments was performed as follows: Random sampling (meander-based sampling) of three digital images (5x objective) per H&E-stained slide was performed for all 20 tissue specimens using the VIS Image Analysis Software. Two independent observers (MFBN and MDS) manually outlined ROIs on the sampled images according to the abovementioned

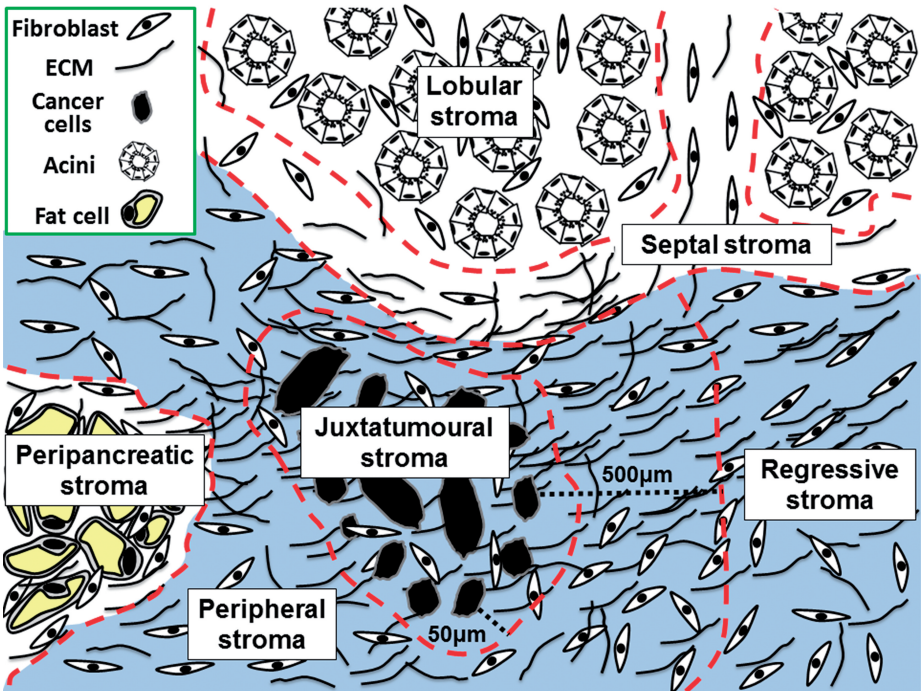

Fig. 1. Simplified, schematic depiction of six stromal compartments in surgical specimens with PC after neoadjuvant treatment (NAT-PC). We modified a previous definition, also taking into account the compartment consisting of regressive stroma (Nielsen et al., 2018). The intratumoural compartments (juxtatumoural, peripheral and regressive stroma) were considered to represent the tumour per se, while the peritumoural compartments (lobular, septal, peri-pancreatic stroma) were considered compartments that surrounded the tumour. This figure is modified from Nielsen et al. (2018). Typing of pancreatic cancer-associated fibroblasts identifies different subpopulations. World Journal of Gastroenterology; 24 (41):4663-4678. With permission from Baishideng Publishing Group.

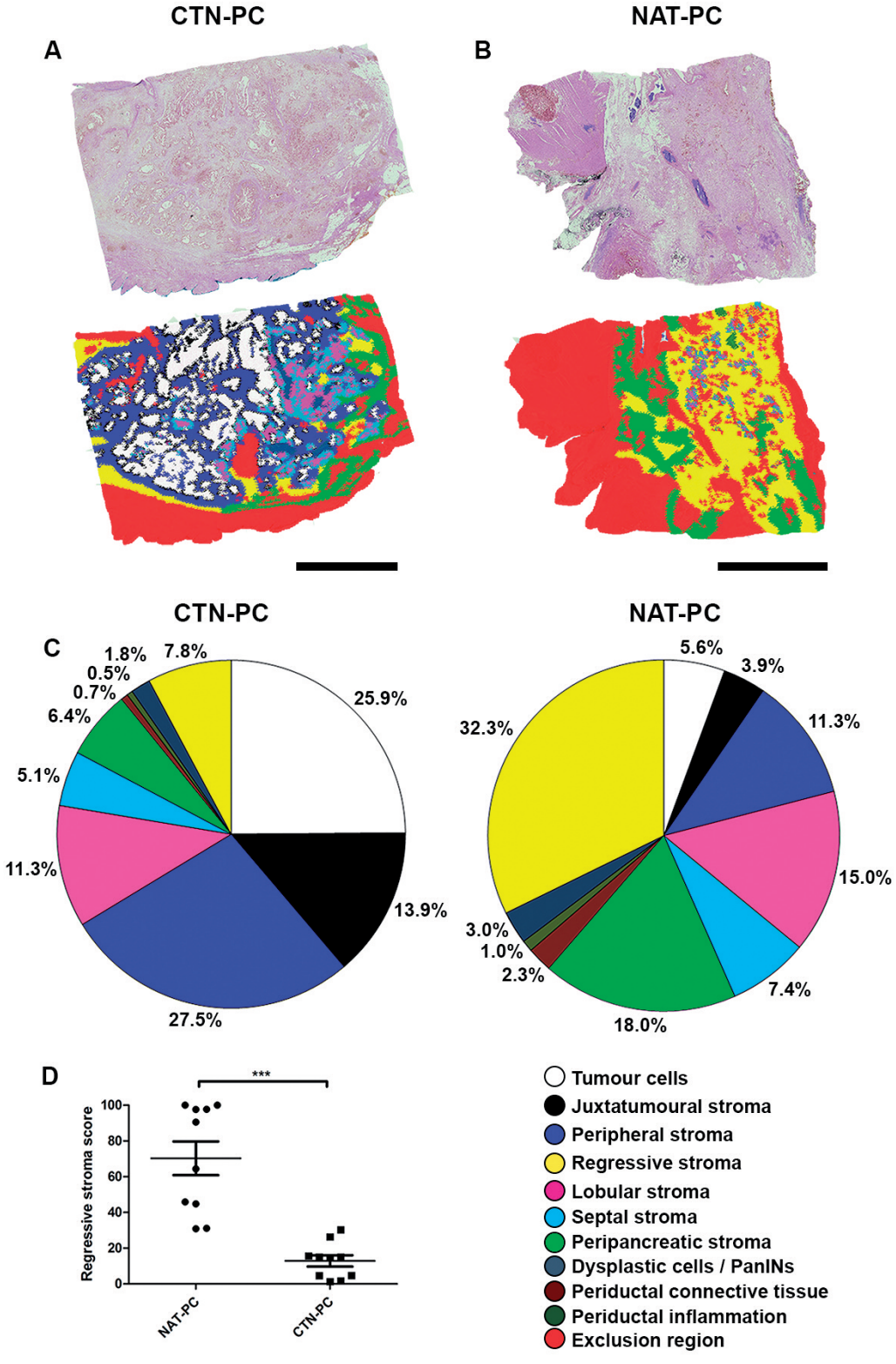

Fig. 2. The regressive stroma fractions in NAT-PC and CTN-PC specimens. Digitalized H&E sections of CTN-PC **(A)** and NAT-PC **(B)** specimens were imported into the Visiopharm software (upper part). Regions of the six stromal compartments (juxtatumoural, peripheral, regressive, lobular, septal, and peripancreatic stroma), tumour cells, periductal connective tissue, periductal inflammation, and dysplastic cells/PanINs were manually outlined and defined as regions of interest (ROIs) (lower part). Fat tissue, blood vessels, nerves, duodenum, lymph nodes and the common bile duct were combined into one region that was defined as an exclusion region, i.e., that was not included in the total ROI. **C.** Pie charts illustrating the area fractions of the different compartments of the total ROI in ten NAT-PC and ten CTN-PC specimens. **D.** The mean regressive stroma fractions (SEM) were 70.3 (9.5) in the 10 NAT-PC specimens and 12.9 (3.2) in the 10 CTN-PC specimens. The regressive stroma fractions were significantly higher in the NAT-PC group than in the CTN-PC group. ***P<0.001. CTN-PC: chemotherapy-naïve pancreatic cancer, NAT-PC: neoadjuvantly treated pancreatic cancer, PanIN: Pancreatic intraepithelial neoplasia, ROI: region of interest. Scale bars: A, 6.5 mm; B, 8.5 mm.

definitions. Areas were determined using the VIS Image Analysis Software for subsequent RS calculations.

Semiquantitative evaluation of IHC and ISH markers

Stained slides were scanned using a 40x objective on a NanoZoomer 2.0HT whole-slide scanner (Hamamatsu Photonics, Hamamatsu, Japan). All quantitative evaluation was performed on digitalized slides using NanoZoomer Digital Pathology (NDP).view2 software (Hamamatsu Photonics).

IHC and ISH stains were assessed using a semiquantitative scoring system, as described previously (Nielsen et al., 2018). Briefly, the expression of each individual marker was assessed in myofibroblasts (MFBs) and ECM in the juxtatumoural, peripheral, lobular, septal, peripancreatic, and regressive stroma using a labelling score (LS) from 0 to 4. In this LS scale, 0 indicated no expression, 1 indicated barely detectable expression, 2 indicated weak expression, 3 indicated moderate expression, and 4 indicated strong expression. Each score was based on the intensity as well as the distribution of the respective marker. α-SMA was used as a reference marker for MFBs, and Sirius Red was used as a reference stain for ECM.

Automated digital image analysis based quantitation of IHC and ISH markers

For validation of the semiquantitative evaluation of IHC and ISH markers, automated DIA and quantitation were performed using VIS Image Analysis Software, version 2018.4. Briefly, ROIs containing juxtatumoural, peripheral, and regressive stroma were manually outlined, according to the definitions described above, in 5 NAT-PC and 5 CTN-PC tissue specimens followed by random sampling (meander-based sampling) of 10 digital images (20x objective) per marker per compartment in each specimen. CD271, cytoglobin, DOG1, miR-21, tenascin C, PDGF-Rβ, and osteonectin expression then were quantified by developing pixel-based algorithms to detect immunopositive staining signals. The method used for each algorithm was threshold-based classification using a hematoxylin/DAB and DAB (HDAB-DAB) feature or a Contrast Red-Blue feature from the RGB colour band. For each marker, the mean intensity and area fraction (defined as the immunopositive area as a fraction of the total area of specific ROI) was quantified. The labelling score for each marker was defined as the product of the area fraction and mean intensity.

Statistical analysis

Pie charts illustrating the area fraction of each of the different compartments of the total ROI were constructed in Microsoft Excel 2010 (Microsoft, Redmond, US). Statistical analysis of the RSs was performed in GraphPad Prism, ver. 5.01 (GraphPad Software, La Jolla, CA, USA). Scatter plots were constructed in GraphPad Prism, ver. 5.01, illustrating the mean RS with the standard error of the mean (SEM). The Mann-Whitney test was used to compare the RSs of CTN-PC with NAT-PC. To correlate the RS with the pathological TRG evaluation, a linear regression analysis was performed in GraphPad Prism, ver. 5.01. Pearson's correlation coefficient (r) and the R squared value (R^2) were calculated to determine how well the data fitted the regression line.

The mean labelling score (MLS) for CD271, cytoglobin, DOG1, miR-21, osteonectin, PDGF-Rβ, or tenascin C was calculated from the average LS. Scatter plots were constructed in GraphPad Prism, ver. 5.01, illustrating the MLS with the SEM. The Mann-Whitney test was used to compare the compartmentalized expression of the markers in CTN-PC versus NAT-PC. Ordinal data were compared using the nonparametric Kruskal-Wallis test followed by Dunn's multiple comparisons test for comparisons of marker expression in the juxtatumoural, peripheral, and regressive stroma.

Evaluation of interrater agreement for quantification of stromal compartments was performed by calculating Fleiss' kappa in GraphPad Prism, quickcalcs online tool (GraphPad Software, San Diego, CA, USA). RSs were divided in 10 different categories representing 10-point intervals (RS 0-10, 10-20, etc.) and Fleiss' kappa was calculated by comparing the data from the two independent observers. The level of statistical significance was set at $P<0.05$. In the graphs, * indicated $P<0.05$, ** indicated $P<0.01$, and *** indicated $P<0.001$.

Results

Quantification of the different stromal compartments in NAT-PC and CTN-PC

Quantitative data of the stromal compartments are presented in Fig. 2A-C. When the compartments of the CTN-PC specimens (Fig. 2A) were compared with those of the NAT-PC specimens (Fig. 2B), the area fraction of the regressive stroma was found to be higher in NAT-PC than in CTN-PC (32.3% vs 7.8%, $P<0.0001$) (Fig. 2C). Conversely, the area fractions of tumour cells (5.6% vs 24.9%, $P=0.002$), juxtatumoural stroma (3.9% vs 13.9%, $P=0.003$), and peripheral stroma (11.3% vs 27.5%, $P=0.03$) were smaller in the NAT-PC specimens than in the CTN-PC specimens, respectively (Fig. 2C).

The RSs for the individual PC specimens were calculated from the juxtatumoural, peripheral and regressive areas (Table 4). The mean RSs of the NAT-PC and CTN-PC specimens were 70.3 (range 30.9-100) and 12.9 (range 1.3-30.3), respectively. Interobserver variability analyses of identification and quantification of stromal compartments demonstrated a very good strength of agreement between two independent observers ($\varkappa=0.85$, Table 5). The comparison of the RS of CTN-PC with that of NAT-PC demonstrated that the RS was significantly higher in NAT-PC than in CTN-PC

(P=0.0002) (Fig. 2D). The RS was further validated by comparing it to a score determined with a conventional histopathological TRG scoring system (modified version of the CAP TRG system) (Washington et al., 2013). The TRG scores for each individual specimen are listed in Table 4. Correlation analyses demonstrated that the RS correlated strongly with the TRG (r=-0.93, R^2=0.86, p<0.0001) (Fig. 3).

Evaluation of the marker phenotype of the different stromal compartments in CTN-PC and NAT-PC

IHC expression of CD271, cytoglobin, DOG1, osteonectin, PDGF-Rβ, and tenascin C and ISH of miR-21 were semiquantitatively evaluated using a four-tiered scoring system to characterize these markers in the juxtatumoural, peripheral, regressive, lobular, septal, and peripancreatic stroma. For validation, automated DIA was used (Fig. 5). The detailed results for each specific compartment are summarized in Table 6.

When evaluating the expression of each of the seven

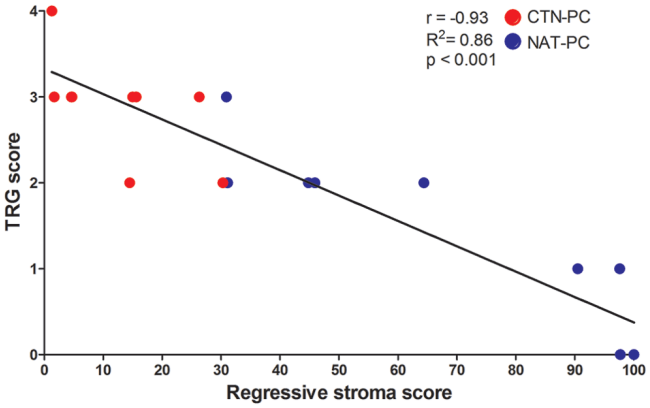

Fig. 3. Correlation between the regressive stroma fraction and TRG score. Linear regression and correlation analyses demonstrated a significant correlation (r=-0.93, R^2=0.86, p<0.0001) between two different methods to evaluate the amount of regressive stroma in pancreatic cancer (PC) specimens. The histological tumour regression grading (TRG) score is shown on the y-axis, and the regressive stroma fraction is on the x-axis.

Table 4. Areal quantification and histological tumour regression grading (TRG) in neoadjuvantly treated pancreatic cancer (NAT-PC) and chemotherapy-naïve pancreatic cancer (CTN-PC).

Nb	Tumour cells Area (mm^2)	Juxtatumoural stroma Area (mm^2)	Peripheral stroma Area (mm^2)	Lobular stroma Area (mm^2)	Septal stroma Area (mm^2)	Peripancreatic stroma Area (mm^2)	Periductal connective tissue Area (mm^2)	Periductal inflammation Area (mm^2)	Dysplastic cells/ PanINs Area (mm^2)	Regressive stroma Area (mm^2)	Excluded region Area (mm^2)	Total region of interest Area (mm^2)	Regressive stroma fraction (0-100)	TRG score (0-4)
NAT-PC group														
1	0.00	0.00	0.00	1.74	3.33	45.52	0.00	0.93	0.00	106.71	172.64	158.23	100	0
2	0.00	0.00	0.00	0.82	1.34	40.23	0.00	0.00	0.00	42.61	133.40	85.0	100	0
3	0.28	0.26	0.48	29.63	13.73	22.91	1.34	0.11	0.43	31.26	235.71	100.42	97.7	0
4	17.92	9.71	17.93	79.20	18.06	9.05	1.89	0.00	0.42	23.47	63.83	177.64	45.9	2
5	6.88	3.79	19.68	53.05	23.37	9.77	2.44	8.39	26.14	42.57	124.56	196.09	64.4	2
6	2.46	4.84	32.99	8.80	6.36	24.22	0.09	0.19	2.54	30.70	195.37	113.18	44.8	2
7	27.11	15.11	30.52	3.65	3.11	15.42	0.94	0.00	2.49	20.42	216.90	118.78	30.9	3
8	13.49	14.05	34.42	0.94	0.70	11.33	0.00	0.40	1.22	21.88	74.82	98.43	31.1	2
9	0.06	0.12	1.32	4.19	18.96	40.14	21.40	2.68	3.73	58.95	213.10	151.54	97.6	1
10	0.21	0.15	1.35	0.83	1.49	0.18	0.00	0.00	0.01	14.34	1.96	18.56	90.5	1
CTN-PC group														
1	15.16	18.60	68.50	2.44	2.94	16.76	0.00	0.00	1.53	15.31	140.27	141.22	15.0	3
2	59.34	22.05	19.11	1.43	0.80	1.73	0.14	0.11	0.88	0.71	200.53	106.3	1.7	3
3	19.50	12.95	15.95	46.36	20.75	9.80	6.41	1.14	0.95	1.41	124.27	135.21	4.7	3
4	43.40	20.17	52.96	13.34	12.38	18.01	1.52	0.00	4.73	12.94	51.52	179.46	15.0	3
5	21.34	19.62	20.63	57.74	9.04	0.00	1.05	0.01	0.17	1.94	126.52	131.55	4.6	3
6	6.86	11.64	66.31	0.34	0.88	15.40	0.08	7.77	4.72	13.26	103.66	127.27	14.5	2
7	100.58	37.31	48.22	10.71	2.96	0.00	0.94	0.02	1.63	1.12	1.93	203.49	1.3	4
8	59.51	28.58	51.56	30.57	15.95	18.35	0.76	0.00	3.21	14.76	103.39	223.25	15.6	3
9	52.56	39.47	75.02	9.50	6.36	15.29	0.00	0.00	1.54	40.90	92.88	240.64	26.3	3
10	38.29	22.30	42.62	17.31	13.77	11.33	0.21	0.00	11.49	28.27	56.96	185.59	30.3	2

The stromal compartments were manually outlined on digitalized slides using Visiopharm software for area quantification. The regressive stroma fraction (RS) was calculated by dividing the area of regressive stroma by the sum of the area of the juxtatumoural, peripheral and regressive stroma multiplied by 100. TRG scores were assessed by a trained pancreatic pathologist using a modification of the CAP TRG system. CAP: College of American Pathologists.

markers mentioned above, no difference was found when the stromal compartments were individually compared between NAT-PC and CTN-PC (Fig. 4). This suggested that NAT does not affect the biomarker profile in the individual compartments. However, as shown in Fig. 2, the amount of regressive stroma was much larger in NAT-PC than in CTN-PC. Thus, for subsequent analyses, we combined the compartmentalized expression data from the NAT-PC and CTN-PC specimens. In general, semiquantitative evaluation and automated DIA-based quantitation of IHC and ISH markers displayed the same compartmentalized expression profiles of the examined markers (Fig. 5). CD271 expression was significantly higher in peripheral than in juxtatumoural CAFs (P<0.01) (Fig. 5A1-5A4). The expression of CD271 in regressive CAFs was moderate/strong (Fig. 5A2). There was no significant difference in the expression of CD271 in regressive and peripheral CAFs, but CD271 expression was significantly higher in regressive CAFs than in juxtatumoural CAFs (P<0.001) (Fig. 5A3-5A4).

In contrast to CD271, the cytoglobin (P<0.05) (Fig.

Table 5. Evaluation of interobserver variability for digital imaging analysis (DIA)-based quantification of stromal compartments.

		Observer 1										
	RS	0-10	10-20	20-30	30-40	40-50	50-60	60-70	70-80	80-90	90-100	Total
Observer 2	0-10	5	0	1	0	0	0	0	0	0	0	6
	10-20	2	0	0	0	0	0	0	0	0	0	2
	20-30	1	0	0	0	0	0	0	0	0	0	1
	30-40	0	0	0	0	1	0	0	0	0	0	1
	40-50	0	0	0	0	0	0	0	0	0	0	0
	50-60	0	0	0	0	1	2	0	0	0	0	3
	60-70	0	0	0	0	1	0	0	0	0	0	1
	70-80	0	0	0	0	0	0	1	0	0	0	1
	80-90	0	0	0	0	0	0	0	0	0	0	0
	90-100	0	0	0	0	0	0	0	0	1	4	5
	Total	8	0	1	0	3	2	1	0	1	4	20

The stromal compartments were manually outlined on digitalized slides using Visiopharm software for area quantification. Two independent observers re-evaluated all 20 included PC tissue specimens. Area quantification of stromal compartments was performed for subsequent calculation of regressive stroma fractions (RS). Interobserver agreement was evaluated by calculating Fleiss' kappa. Weighted κ: 0.850. Strength of agreement: Very good.

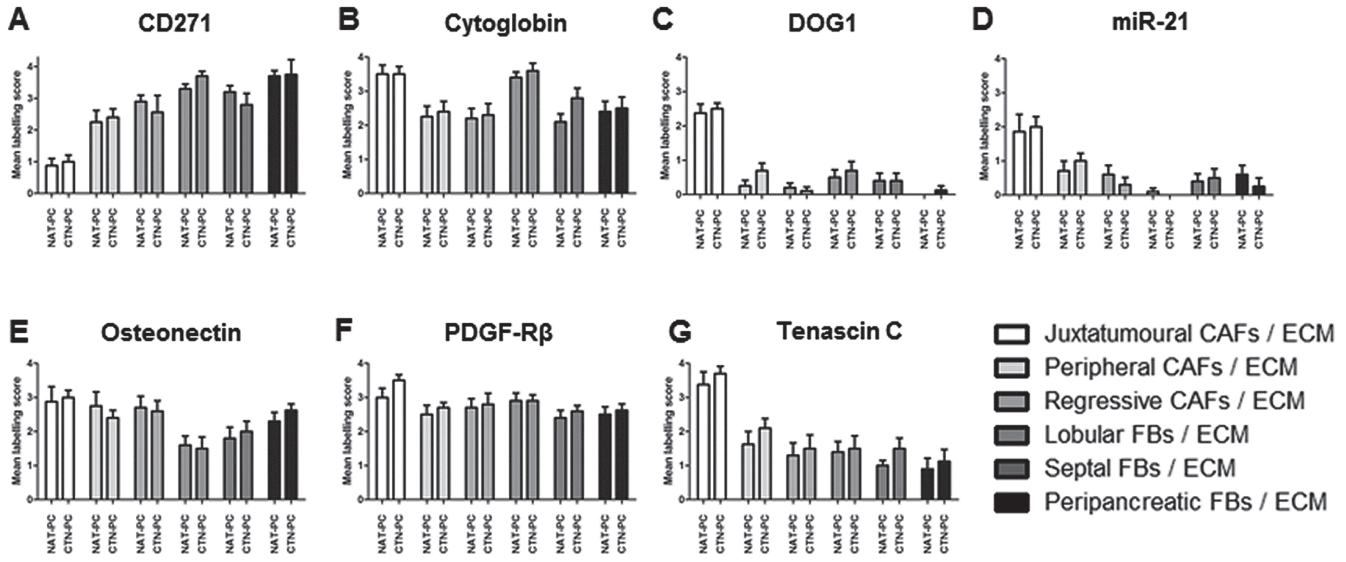

Fig. 4. Comparison of the compartmentalized marker profile of neoadjuvantly treated pancreatic cancer (NAT-PC) compared to that of chemotherapy-naïve pancreatic cancer (CTN-PC). The expression levels of CD271 **(A)**, cytoglobin **(B)**, DOG1 **(C)**, miR-21 **(D)**, osteonectin **(E)**, PDGF-Rβ **(F)**, and tenascin C **(G)** were semiquantitatively evaluated separately in NAT-PC and CTN-PC specimens in the juxtatumoural, peripheral, regressive, lobular, septal, and peripancreatic cancer-associated fibroblasts (CAFs), fibroblasts (FBs) and extracellular matrix (ECM). Statistical analyses demonstrated that there were no statistically significant differences in the expression of any marker when the expression of each was examined in each specific compartment in NAT-PC versus CTN-PC. The graphs illustrate mean labelling scores (MLS) with standard error of the mean (SEM). DOG1: discovered on gastrointestinal stromal tumours 1. PDGF-Rβ: platelet-derived growth factor receptor β.

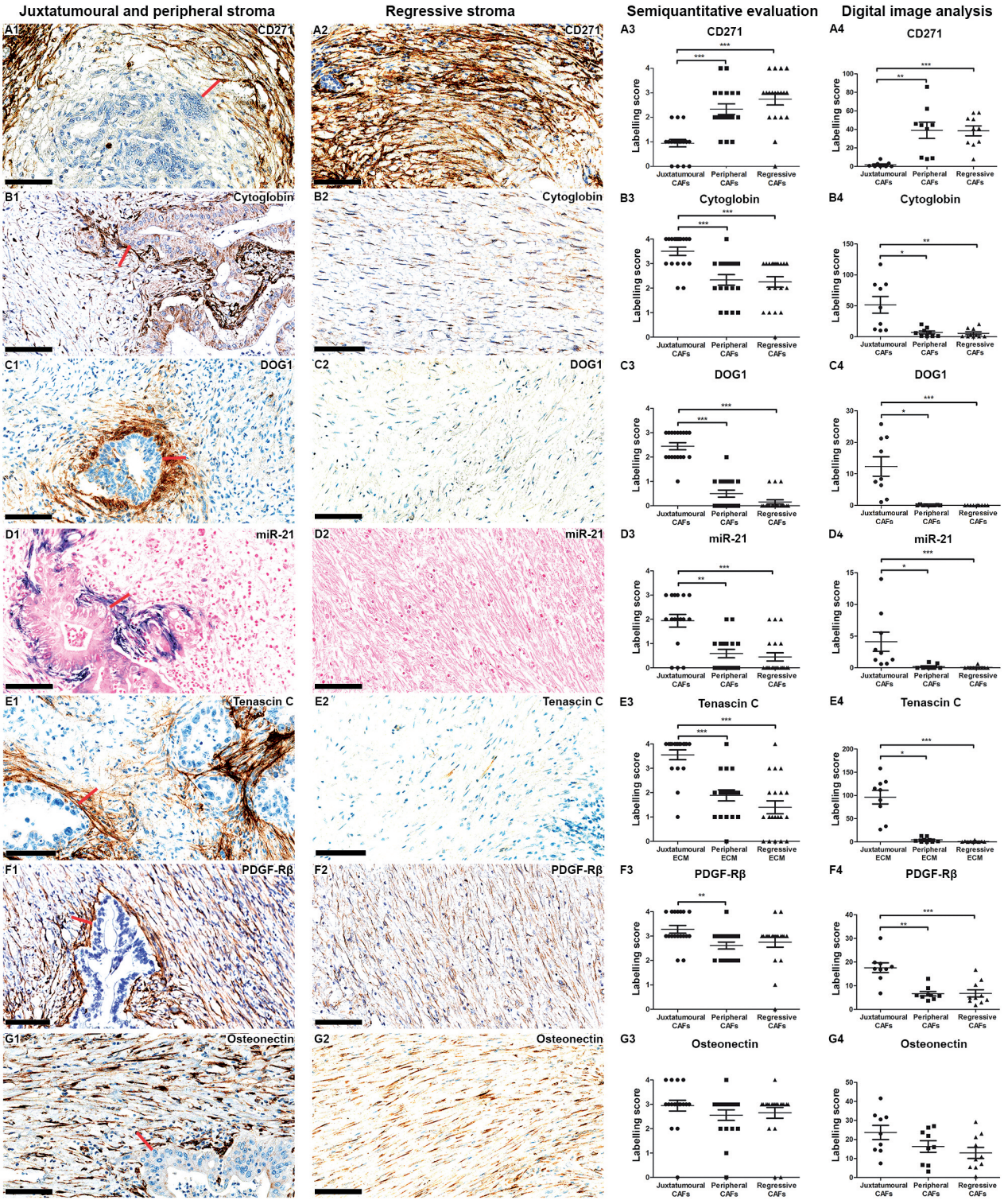

Fig. 5. Immunohistochemical (IHC) expression of CD271 **(A1-A4)**, cytoglobin **(B1-B4)**, DOG1 **(C1-C4)**, miR-21 **(D1-D4)**, tenascin C **(E1-E4)**, PDGF-Rβ **(F1-F4)**, and osteonectin **(G1-G4)** in cancer-associated fibroblasts (CAFs) and extracellular matrix (ECM) in the juxtatumoural, peripheral, and regressive stroma in pancreatic cancer, evaluated semiquantitatively (SE) and using automated digital image analysis (DIA). **A1-A4.** CD271 was weakly expressed in juxtatumoural CAFs (mean labelling score (MLS (SE))=0.9, (MLS (DIA))=1.8) but highly expressed in peripheral CAFs (MLS (SE)=2.3, MLS (DIA)=39.0) and regressive CAFs (MLS (SE)=2.7, MLS (DIA)=38.4). **B1-B4.** Cytoglobin was highly expressed in juxtatumoural CAFs (MLS (SE)=3.5, MLS (DIA)=51.6) with lower expression levels in peripheral CAFs (MLS (SE)=2.3, MLS (DIA)=7.0) and regressive CAFs (MLS (SE)=2.3, MLS (DIA)=5.6). **C1-C4.** DOG1 expression was high in juxtatumoural CAFs (MLS (SE)=2.4, MLS (DIA)=12.3), but almost absent in peripheral CAFs (MLS (SE)=0.5, MLS (DIA)=0.1) and regressive CAFs (MLS (SE)=0.2, MLS (DIA)=0.03). **D1-D4.** Moderate miR-21 expression was observed in juxtatumoural CAFs (MLS (SE)=1.9, MLS (DIA)=4.1), and miR-21 expression was mostly absent in peripheral CAFs (MLS (SE)=0.6, MLS (DIA)=0.2) and regressive CAFs (MLS (SE)=0.5, MLS (DIA)=0.1). (E1-E4) Tenascin C was strongly expressed in the juxtatumoural ECM (MLS (SE)=3.6, MLS (DIA)=96.4), weakly expressed in the peripheral ECM (MLS (SE)=1.9, MLS (DIA)=4.4) and almost undetectable in the regressive ECM (MLS (SE)=1.4, MLS (DIA)=1.0). **F1-F4.** PDGF-Rβ expression was strong in juxtatumoural CAFs (MLS (SE)=3.3, MLS (DIA)=17.6) and moderate in peripheral CAFs (MLS (SE)=2.6, MLS (DIA)=6.6) and regressive CAFs (MLS (SE)=2.8, MLS (DIA)=6.8). **G1-G4.** Osteonectin was moderately expressed in all three CAF subtypes: juxtatumoural CAFs (MLS (SE)=2.9, MLS (DIA)=23.7), peripheral CAFs (MLS (SE)=2.6, MLS (DIA)=16.3), and regressive CAFs (MLS (SE)=2.7, MLS (DIA)=13.0). * indicates P<0.05, ** indicates P<0.01, and *** indicates P<0.001. Scale bars: Black, 100 μm; Red, 50 μm.

5B1-5B4), DOG1 (P<0.05) (Fig. 5C1-5C4), and miR-21 (P<0.05) (Fig. 5D1-5D4) expression levels were all significantly higher in juxtatumoural than in peripheral and regressive CAFs. There were no significant differences in the expression levels of these markers in peripheral compared to those in regressive CAFs. Tenascin C was strongly expressed in juxtatumoural ECM, and its expression was significantly higher in juxtatumoural than in peripheral and regressive ECM (P<0.05) (Fig. 5E1-5E4). The expression of tenascin C in peripheral ECM did not differ significantly from that in regressive ECM.

PDGF-Rβ expression was most prominent in the juxtatumoural stroma but was also moderate/strong in both the peripheral and regressive stroma (Fig. 5F1-5F4). When the expression of PDGF-Rβ was compared between the compartments, it was found to be significantly higher in juxtatumoural than in peripheral CAFs (P<0.01), whereas no significant differences were observed between regressive CAFs and the other two CAF subtypes based on the semiquantitative evaluation (Fig. 5F3), while PDGF-Rβ expression was significantly higher in juxtatumoural than in regressive CAFs based on DIA (P<0.001) (Fig. 5F4). Osteonectin displayed moderate expression in all three compartments, and there were no significant differences among juxtatumoural, peripheral, and regressive CAFs (Fig. 5G1-5G4).

A summary of the compartmentalized expression profile of the seven markers is listed in Table 7. Among the tumoural compartments, the antigen expression of CD271, cytoglobin, miR-21, PDGF-Rβ, and tenascin C in the regressive stroma was highly similar to the peripheral and different from the juxtatumoural stroma. Furthermore, while the juxtatumoural stroma was characterized by moderate DOG1 expression, this marker was only barely perceptible in the peripheral and absent in the regressive stroma. Regarding the peritumoural compartments (lobular, septal and peripancreatic stroma), the antigen expression profiles were generally very similar (Fig. 4, Table 7). The only notable exception was cytoglobin, a marker that was expressed strongly in the lobular stroma, similar to the juxtatumoural stroma but different from the remaining compartments, where only weak cytoglobin expression was found. In summary, the marker phenotype of regressive CAFs and regressive ECM was similar to peripheral CAFs and peripheral ECM ($CD271^{high}$, $cytoglobin^{low}$, $DOG1^{low}$, $miR\text{-}21^{low}$, $PDGF\text{-}R\beta^{low}$, and tenascin C^{low}). Furthermore, the marker profiles of regressive CAFs and regressive ECM differed from the marker profiles of juxtatumoural CAFs and juxtatumoural ECM ($CD271^{low}$, $cytoglobin^{high}$, $DOG1^{high}$, $miR\text{-}21^{high}$, $PDGF\text{-}R\beta^{high}$, and tenascin C^{high}). Juxtatumoural CAFs and juxtatumoural ECM, on the other hand, differed from all other compartments by the following antigen expression profile: $CD271^{low}$, $DOG1^{high}$, $miR\text{-}21^{high}$, $PDGF\text{-}R\beta^{high}$, and tenascin C^{high}.

Discussion

In this study, we characterized the marker phenotypic properties of the regressive stroma in NAT-PC and compared it with the juxtatumoural and peripheral stroma that is found in CTN-PC. We found that the amount of regressive stroma was much higher in NAT-PC compared to CTN-PC. This was found

Table 6. Semiquantitative evaluation of the expression of seven markers in cancer-associated fibroblasts (CAFs) and extracellular matrix (ECM) in the juxtatumoural, peripheral, regressive, lobular, septal, and peripancreatic stroma of neoadjuvantly treated pancreatic cancer (NAT-PC) and chemotherapy-naïve pancreatic cancer (CTN-PC).

Marker	Juxtatumoural stroma MLS (SEM)	Peripheral stroma MLS (SEM)	Regressive stroma MLS (SEM)	Lobular stroma MLS (SEM)	Septal stroma MLS (SEM)	Peripancreatic stroma MLS (SEM)
NAT-PC						
CD271	0.88 (0.23)	2.25 (0.37)	2.89 (0.20)	3.30 (0.15)	3.20 (0.20)	2.90 (0.18)
Cytoglobin	3.50 (0.27)	2.25 (0.31)	2.20 (0.29)	3.40 (0.16)	2.10 (0.23)	2.40 (0.31)
DOG1	2.38 (0.26)	0.25 (0.16)	0.20 (0.13)	0.50 (0.22)	0.40 (0.22)	0.0 (0.0)
miR-21	1.86 (0.51)	0.71 (0.29)	0.60 (0.27)	0.1 (0.1)	0.40 (0.22)	0.60 (0.27)
Osteonectin	2.88 (0.44)	2.75 (0.41)	2.70 (0.34)	1.60 (0.27)	1.80 (0.33)	2.30 (0.26)
PDGF-Rβ	3.0 (0.27)	2.50 (0.27)	2.70 (0.26)	2.90 (0.23)	2.40 (0.22)	2.50 (0.22)
Tenascin C	3.38 (0.38)	1.63 (0.38)	1.30 (0.37)	1.40 (0.31)	1.0 (0.15)	0.90 (0.31)
CTN-PC						
CD271	1.0 (0.21)	2.40 (0.27	2.50 (0.53)	3.70 (0.15)	2.80 (0.36)	2.56 (0.47)
Cytoglobin	3.50 (0.22)	2.40 (0.31)	2.30 (0.34)	3.60 (0.22)	2.80 (0.29)	2.50 (0.33)
DOG1	2.50 (0.17)	0.70 (0.21)	0.11 (0.11)	0.70 (0.26)	0.40 (0.22)	0.13 (0.13)
miR-21	2.0 (0.30)	0.50 (0.22)	0.30 (0.21)	0.0 (0.0)	0.50 (0.27)	0.25 (0.25)
Osteonectin	3.0 (0.21)	2.40 (0.22)	2.60 (0.31)	1.50 (0.34)	2.0 (0.30)	2.63 (0.18)
PDGF-Rβ	3.50 (0.17)	2.70 (0.15)	2.80 (0.33)	2.90 (0.18)	2.60 (0.16)	2.63 (0.18)
Tenascin C	3.70 (0.21)	2.10 (0.28)	1.50 (0.40)	1.50 (0.37)	1.50 (0.31)	1.13 (0.35)

CD: cluster of differentiation, DOG1: discovered on gastrointestinal stromal tumours 1, MLS: mean labelling score, PDGF-Rβ: platelet-derived growth factor receptor β, SEM: standard error of the mean.

semiquantitatively by manual scoring and also when using digital imaging analysis (DIA), supporting the utility of our method to identify the regressive stroma in PC. Next, we examined the marker phenotype of CAFs in the regressive stroma, with special emphasis on similarities or dissimilarities with juxtatumoural and peripheral CAFs. We found that the antigen expression characteristics of regressive CAFs were similar to those of peripheral CAFs, which are located at a greater distance from the cancer cells, and different from those of juxtatumoural CAFs, which are located in close vicinity to the cancer cells. Moreover, the present study confirms that different subtypes of CAFs with different antigen expression exist in PC. Moreover, our data provide indirect support of the hypothesis that phenotypically different subtypes of CAFs, at least in part, also may hold different functional properties (Iacobuzio-Donahue et al., 2002; Öhlund et al., 2017; Nielsen et al., 2018).

Only a few studies have examined the marker phenotypic properties of the regressive stroma in PC. One study described the intratumour stromal expression of tenascin C in resected PC specimens after receiving chemoradiation therapy (CRT), using either a gemcitabine-based or a S-1 (tegafur, gimeracil and oteracil) and gemcitabine-based protocol (Hayasaki et al., 2018). After dividing the patients in high and low responder groups according to the Evans grading system (Evans et al., 1992), the intratumour stromal expression of tenascin C was significantly higher in low responders than in high responders (Hayasaki et al., 2018). This finding is in line with our results, as the phenotypic signature of regressive stroma was characterized by low expression of tenascin C compared to that of the juxtatumoural stroma. It may be speculated that markers such as CD271, cytoglobin, DOG1, and miR-21 could also aid in the evaluation of response to NAT along with tenascin C. A published abstract reported the expression of tenascin C in PC resection specimens after preoperative chemotherapy or CRT, along with other IHC markers, such as pan-cytokeratin, α-crystallin B, α-SMA, neurotrophin-3, Ki-67, and osteonectin (Haeberle et al., 2017). The authors concluded that differentiating between the desmoplastic stroma and the regressive stroma based on the examined list of markers is very challenging. However, it seems that the juxtatumoural and peripheral tumour stroma were not examined separately in this study. Another study focused on the CAF density in the regressive stroma (Miyashita et al., 2018). NAT with gemcitabine and nab-paclitaxel resulted in a reduction of the total number of CAFs. Together with our own results, these data highlight that NAT may affect not only the phenotypic composition of CAFs but also the overall number of CAFs in the PC stroma.

Stromal compartmentalization is not a novel concept in PC. A study from 2002 used ISH and found that three genes (MMP11, Apolipoprotein C-1 and Apolipoprotein D) were expressed in the juxtatumoural stroma only (Iacobuzio-Donahue et al., 2002). In a later study in mice, the markers α-SMA, neuron-glial antigen 2 (NG2), PDGF-Rβ, and S100A4 indicated a mixed population of CAFs in the tumour microenvironment (Sugimoto et al., 2006). More recent studies also support the concept of stromal compartmentalization in PC, demonstrating prominent expression of fibroblast activation protein (FAP), α-SMA, NT-3, osteonectin, and tenascin C in the perilesional (= juxtatumoural) compartment (Öhlund et al., 2017; Haeberle et al., 2018). Moreover, CD10, cytoglobin, DOG1, nestin, miR-21, and tenascin C could be used to distinguish the marker phenotype of the juxtatumoural from that of the peripheral stroma (Nielsen et al., 2018). The signature of the lobular and septal fibroblasts (FBs) was less pronounced, but lobular FBs were characterized by a high expression of cytoglobin and CD271, and the septal FBs by a high expression of CD271 (Nielsen et al., 2018).

Stromal heterogeneity may in part explain the

Table 7. Simplified scheme of the expression profiles of CD271, cytoglobin, DOG1, miR-21, osteonectin, PDGF-Rβ, and tenascin C in different stromal compartments of neoadjuvantly treated and chemotherapy-naïve pancreatic cancer.

	Fibroblast markers						ECM marker
	CD271	Cytoglobin	DOG1	miR-21	Osteonectin	PDGF-Rβ	Tenascin C
Intratumoural compartments							
Juxtatumoural stroma	+	++++	+++	+++	+++	++++	++++
Peripheral stroma	+++	++	+	+	+++	++	+
Regressive stroma	+++	++	-	+	+++	++	+
Peritumoural compartments							
Lobular stroma	++++	++++	+	-	++	+++	+
Septal stroma	+++	++	-	+	+++	+++	+
Peripancreatic stroma	++++	++	-	+	+++	+++	+

The intratumoural compartments (juxtatumoural, peripheral and regressive stroma) represent the tumour per se, while the peritumoural compartments (lobular, septal, peripancreatic stroma) represent compartments that surround the tumour. Symbol key: (-) Not expressed in the cell type; (+) barely detectable expression; (++) weak expression; (+++) moderate expression; (++++) strong expression. DOG1: discovered on gastrointestinal stromal tumours 1, ECM: extracellular matrix, PDGF-Rβ: platelet-derived growth factor receptor β.

previously published, and partially contradictory, reports on the role of the tumour stroma in PC progression. While high numbers of α-SMA-positive CAFs were reported to hold negative prognostic value in human PC and while CAFs were found to constrain the effect of CRT while supporting tumour progression, depletion of the whole population of CAFs was associated with tumour progression and reduced survival in mice (Erkan et al., 2008; Hwang et al., 2008; Vonlaufen et al., 2008a; Mantoni et al., 2011; Rhim et al., 2014; Özdemir et al., 2014). It has been suggested that (some of the) juxtatumoural CAFs, located in close contact with PC cells, may play a supportive role in PC progression, in contrast to (some of the) CAFs located at a greater distance from cancer cells (peripheral CAFs) (Iacobuzio-Donahue et al., 2002; Nielsen et al., 2018). In the present study, the marker phenotypic signature of regressive CAFs in neoadjuvantly treated PC was similar to that of peripheral CAFs, supporting the hypothesis that these cells also, at least in part, may share functional properties. It is tempting to speculate that juxtatumoural CAFs may also be destroyed in tumour areas where NAT effectively eliminates PC cells (= in the regressive stroma). An obvious alternative hypothesis could be that NAT changes the functional (and marker phenotypic) properties of juxtatumoural CAFs to a peripheral CAF-/regressive CAF-like type of cell. Taken together, it is tempting to speculate that our findings may support the proposed close association between juxtatumoural CAFs and PC cells, as indicated by several studies (Bachem et al., 2005; Hwang et al., 2008; Vonlaufen et al., 2008b).

We defined six stromal compartments in resection specimens with PC. One can argue that such an approach is too simplistic when evaluating complex biological conditions. Intra- and inter-tumour heterogeneity further add to the complexity of the PC architecture (Verbeke, 2016). Additionally, one can argue that the appointed cut-off values between compartments (e.g., 500 μm away from cancer cells as the cut-off between the peripheral and regressive stroma) are debatable. However, this strategy provides a framework for separately evaluating stromal compartments, and similar definitions of the stromal compartments in PC have been used in previous studies (Ene-Obong et al., 2013; Nielsen et al., 2018). We and others have previously utilized a cut-off of 100 μm to distinguish the juxtatumoural from the peripheral stroma (Ene-Obong et al., 2013; Nielsen et al., 2018). However, based on the results from our previous study, we concluded that the cut-off between the juxtatumoural and peripheral stroma should rather be 50 μm, and therefore this cut-off was used in the present study (Nielsen et al., 2018).

It can be challenging for pathologists to objectively evaluate histological tumour regression as a response to NAT in PC due to the high amounts of desmoplastic stroma characterizing these neoplasms (Verbeke et al., 2015). Hence, it was crucial for this study to develop a method that allowed us to identify the regressive stroma in NAT-PC specimens. We therefore used two different methods for definition and quantification of the regressive stroma. The NAT-PC specimens contained significantly higher amounts of regressive stroma than the CTN-PC specimens, and there was a highly significant correlation between the two different methods in evaluating the amount of regressive stroma. The methods used were 1) the manual TRG score based on a slightly modified CAP system and 2) manual outlining of the regressive stroma together with five other stromal compartments using DIA (Washington et al., 2013). The utility of this latter technique was strengthened by interobserver variability analyses that demonstrated a very good correlation between two independent observers. These findings supported our approach using stromal compartmentalization for the evaluation of the marker phenotypic properties of regressive stroma. We performed both a semiquantitative evaluation and an automated DIA-based quantitation of IHC and ISH markers that displayed the same compartmentalized expression profiles. Of note, we also identified small quantities of regressive stroma in CTN-PC specimens. This may be due to a host immunological response against tumour cells (Chin et al., 2018). An alternative explanation could be that the cut-off that we used for the differentiation of peripheral stroma from regressive stroma may have been too conservative. Future studies with a higher number of patients are needed to evaluate our method, using varying cut-offs. Such studies should also determine whether this method holds prognostic value in PC after NAT.

In conclusion, our data provide further support of the concept of stromal heterogeneity and the existence of different CAF subtypes in PC. Our findings indicate that the antigen expression of CAFs in the regressive stroma in NAT-PC is similar to that of peripheral CAFs but different from that of juxtatumoural CAFs, supporting the hypothesis that these cells, at least in part, also may share functional properties. It is possible that additional (functional) CAF subtypes may be identified in the future, for example when single-cell transcriptomics is used. Studies evaluating the precise functional properties of CAF subtypes in PC are needed.

Acknowledgements. We are thankful to senior histotechnologist and project coordinator Ole Nielsen and to histotechnologists Lisbet Mortensen, Lone Christiansen, and Christian Enggaard, Department of Pathology, Odense University Hospital, for their assistance with the IHC staining. We thank Claus Fristrup, Department of Surgery, Odense University Hospital, for his advice regarding the statistical analyses. This work was supported by Aase-and-Ejnar Danielsen's Foundation (grant number 10-001452), Brødrene Hartmann's Foundation (grant number A28308), the Foundation of 17.12.1981 (grant number 19024005), Knud og Edith Eriksens Mindefond (grant number 62786), Kong Christian den Tiendes Foundation (grant number 5/2018), the University of Southern Denmark Faulty Scholarship, the Odense University Hospital Free Research Fund (grant numbers 29-A1500, 22-A1133 and 49-A2379), Odense University Hospital PhD stipend (grant number 1032), and Odense Pancreas Center (OPAC).

References

Apte M.V., Haber P.S., Applegate T.L., Norton I.D., McCaughan G.W., Korsten M.A., Pirola R.C. and Wilson J.S. (1998). Periacinar stellate shaped cells in rat pancreas: Identification, isolation, and culture. Gut 43, 128-133.

Bachem M.G., Schunemann M., Ramadani M., Siech M., Beger H., Buck A., Zhou S., Schmid-Kotsas A. and Adler G. (2005). Pancreatic carcinoma cells induce fibrosis by stimulating proliferation and matrix synthesis of stellate cells. Gastroenterology 128, 907-921.

Bachem M.G., Schneider E., Gross H., Weidenbach H., Schmid R.M., Menke A., Siech M., Beger H., Grunert A. and Adler G. (1998). Identification, culture, and characterization of pancreatic stellate cells in rats and humans. Gastroenterology 115, 421-432.

Chatterjee D., Katz M.H., Rashid A., Estrella J.S., Wang H., Varadhachary G.R., Wolff R.A., Lee J.E., Pisters P.W., Abbruzzese J.L., Fleming J.B. and Wang H. (2013). Pancreatic intraepithelial neoplasia and histological changes in non-neoplastic pancreas associated with neoadjuvant therapy in patients with pancreatic ductal adenocarcinoma. Histopathology 63, 841-851.

Chin K.M., Chan C.Y. and Lee S.Y. (2018). Spontaneous regression of pancreatic cancer: A case report and literature review. Int. J. Surg. Case Rep. 42, 55-59.

Dang C., Zhang Y., Ma Q. and Shimahara Y. (2006). Expression of nerve growth factor receptors is correlated with progression and prognosis of human pancreatic cancer. J. Gastroenterol. Hepatol. 21, 850-858.

D.P.C.D. (2017). In. http://www.dpcg.gicancer.dk/.

Ene-Obong A., Clear A.J., Watt J., Wang J., Fatah R., Riches J.C., Marshall J.F., Chin-Aleong J., Chelala C., Gribben J.G., Ramsay A.G. and Kocher H.M. (2013). Activated pancreatic stellate cells sequester cd8+ t cells to reduce their infiltration of the juxtatumoral compartment of pancreatic ductal adenocarcinoma. Gastroenterology 145, 1121-1132.

Erkan M., Michalski C.W., Rieder S., Reiser-Erkan C., Abiatari I., Kolb A., Giese N.A., Esposito I., Friess H. and Kleeff J. (2008). The activated stroma index is a novel and independent prognostic marker in pancreatic ductal adenocarcinoma. Clin. Gastroenterol. Hepatol 6, 1155-1161.

Erkan M., Adler G., Apte M.V., Bachem M.G., Buchholz M., Detlefsen S., Esposito I., Friess H., Gress T.M., Habisch H.J., Hwang R.F., Jaster R., Kleeff J., Kloppel G., Kordes C., Logsdon C.D., Masamune A., Michalski C.W., Oh J., Phillips P.A., Pinzani M., Reiser-Erkan C., Tsukamoto H. and Wilson J. (2012). Stellatum: Current consensus and discussion on pancreatic stellate cell research. Gut 61, 172-178.

Evans D.B., Rich T.A., Byrd D.R., Cleary K.R., Connelly J.H., Levin B., Charnsangavej C., Fenoglio C.J. and Ames F.C. (1992). Preoperative chemoradiation and pancreaticoduodenectomy for adenocarcinoma of the pancreas. Arch. Surg. 127, 1335-1339.

Farrow B., Rowley D., Dang T. and Berger D.H. (2009). Characterization of tumor-derived pancreatic stellate cells. J. Surg. Res 157, 96-102.

Fujiwara K., Ohuchida K., Mizumoto K., Shindo K., Eguchi D., Kozono S., Ikenaga N., Ohtsuka T., Takahata S., Aishima S. and Tanaka M. (2012). Cd271(+) subpopulation of pancreatic stellate cells correlates with prognosis of pancreatic cancer and is regulated by interaction with cancer cells. PLoS One 7, e52682.

Gore J. and Korc M. (2014). Pancreatic cancer stroma: Friend or foe? Cancer Cell 25, 711-712.

Gostimir M., Bennett S., Moyana T., Sekhon H. and Martel G. (2016). Complete pathological response following neoadjuvant folfirinox in borderline resectable pancreatic cancer - a case report and review. BMC Cancer 16, 786.

Haeberle L., Kapp A.-C. and Esposito I. (2017). Morphologic characterization of pancreatic ductal adenocarcinoma after neoadjuvant therapy. Pancreatology 17, S20.

Haeberle L., Steiger K., Schlitter A.M., Safi S.A., Knoefel W.T., Erkan M. and Esposito I. (2018). Stromal heterogeneity in pancreatic cancer and chronic pancreatitis. Pancreatology. 18, 536-549.

Hayasaki A., Murata Y., Usui M., Hibi T., Ito T., Iizawa Y., Kato H., Tanemura A., Azumi Y., Kuriyama N., Kishiwada M., Mizuno S., Sakurai H., Yoshida T. and Isaji S. (2018). Clinical significance of histological effect and intratumor stromal expression of tenascin-c in resected specimens after chemoradiotherapy for initially locally advanced unresectable pancreatic ductal adenocarcinoma. Pancreas 47, 390-399.

Hwang R.F., Moore T., Arumugam T., Ramachandran V., Amos K.D., Rivera A., Ji B., Evans D.B. and Logsdon C.D. (2008). Cancer-associated stromal fibroblasts promote pancreatic tumor progression. Cancer Res. 68, 918-926.

Iacobuzio-Donahue C.A., Ryu B., Hruban R.H. and Kern S.E. (2002). Exploring the host desmoplastic response to pancreatic carcinoma: Gene expression of stromal and neoplastic cells at the site of primary invasion. Am. J. Pathol 160, 91-99.

Ikenaga N., Ohuchida K., Mizumoto K., Cui L., Kayashima T., Morimatsu K., Moriyama T., Nakata K., Fujita H. and Tanaka M. (2010). CD10+ pancreatic stellate cells enhance the progression of pancreatic cancer. Gastroenterology 139, 1041-1051.

Jones T.S., Jones E.L., McManus M., Shah R. and Gajdos C. (2013). Multifocal anaplastic pancreatic carcinoma requiring neoadjuvant chemotherapy and total pancreatectomy: Report of a case. JOP 14, 289-291.

Kadaba R., Birke H., Wang J., Hooper S., Andl C.D., Di M.F., Soylu E., Ghallab M., Bor D., Froeling F.E., Bhattacharya S., Rustgi A.K., Sahai E., Chelala C., Sasieni P. and Kocher H.M. (2013). Imbalance of desmoplastic stromal cell numbers drives aggressive cancer processes. J. Pathol. 230, 107-117.

Kadera B.E., Li L., Toste P.A., Wu N., Adams C., Dawson D.W. and Donahue T.R. (2013). MicroRNA-21 in pancreatic ductal adenocarcinoma tumor-associated fibroblasts promotes metastasis. PLoS. One 8, e71978.

Mantoni T.S., Lunardi S., Al-Assar O., Masamune A. and Brunner T.B. (2011). Pancreatic stellate cells radioprotect pancreatic cancer cells through beta1-integrin signaling. Cancer Res. 71, 3453-3458.

Miyashita T., Tajima H., Makino I., Okazaki M., Yamaguchi T., Ohbatake Y., Nakanuma S., Hayashi H., Takamura H., Ninomiya I., Fushida S., Kishimoto K., Harmon J.W. and Ohta T. (2018). Neoadjuvant chemotherapy with gemcitabine plus nab-paclitaxel reduces the number of cancer-associated fibroblasts through depletion of pancreatic stroma. Anticancer Res. 38, 337-343.

Nielsen B.S., Jørgensen S., Fog J.U., Søkilde R., Christensen I.J., Hansen U., Brünner N., Baker A., Møller S. and Nielsen H.J. (2011). High levels of microRNA-21 in the stroma of colorectal cancers predict short disease-free survival in stage II colon cancer patients. Clin. Exp. Metastasis 28, 27-38.

Nielsen M.F., Mortensen M.B. and Detlefsen S. (2016). Key players in pancreatic cancer-stroma interaction: Cancer-associated fibroblasts,

endothelial and inflammatory cells. World J. Gastroenterol. 22, 2678-2700.

Nielsen M.F.B., Mortensen M.B. and Detlefsen S. (2017). Identification of markers for quiescent pancreatic stellate cells in the normal human pancreas. Histochem. Cell Biol. 148, 359-380.

Nielsen M.F.B., Mortensen M.B. and Detlefsen S. (2018). Typing of pancreatic cancer-associated fibroblasts identifies different subpopulations. World J. Gastroenterol. 24, 4663-4678.

Öhlund D., Handly-Santana A., Biffi G., Elyada E., Almeida A.S., Ponz-Sarvise M., Corbo V., Oni T.E., Hearn S.A., Lee E.J., Chio, II, Hwang C.I., Tiriac H., Baker L.A., Engle D.D., Feig C., Kultti A., Egeblad M., Fearon D.T., Crawford J.M., Clevers H., Park Y. and Tuveson D.A. (2017). Distinct populations of inflammatory fibroblasts and myofibroblasts in pancreatic cancer. J. Exp. Med. 214, 579-596.

Özdemir B.C., Pentcheva-Hoang T., Carstens J.L., Zheng X., Wu C.C., Simpson T.R., Laklai H., Sugimoto H., Kahlert C., Novitskiy S.V., De Jesus-Acosta A., Sharma P., Heidari P., Mahmood U., Chin L., Moses H.L., Weaver V.M., Maitra A., Allison J.P., LeBleu V.S. and Kalluri R. (2014). Depletion of carcinoma-associated fibroblasts and fibrosis induces immunosuppression and accelerates pancreas cancer with reduced survival. Cancer Cell 25, 719-734.

Pai R.K. and Pai R.K. (2018). Pathologic assessment of gastrointestinal tract and pancreatic carcinoma after neoadjuvant therapy. Mod. Pathol. 31, 4-23.

Rhim A.D., Oberstein P.E., Thomas D.H., Mirek E.T., Palermo C.F., Sastra S.A., Dekleva E.N., Saunders T., Becerra C.P., Tattersall I.W., Westphalen C.B., Kitajewski J., Fernandez-Barrena M.G., Fernandez-Zapico M.E., Iacobuzio-Donahue C., Olive K.P. and Stanger B.Z. (2014). Stromal elements act to restrain, rather than support, pancreatic ductal adenocarcinoma. Cancer Cell 25, 735-747.

Sobin L., Gospodarowicz M. and Wittekind C. (2009). TNM classification of malignant tumours, New York: International Union Against Cancer (UICC).

Sugimoto H., Mundel T.M., Kieran M.W. and Kalluri R. (2006). Identification of fibroblast heterogeneity in the tumor microenvironment. Cancer Biol. Ther 5, 1640-1646.

Verbeke C. (2016). Morphological heterogeneity in ductal adenocarcinoma of the pancreas - does it matter? Pancreatology 16, 295-301.

Verbeke C., Löhr M., Karlsson J.S. and Del Chiaro M. (2015). Pathology reporting of pancreatic cancer following neoadjuvant therapy: Challenges and uncertainties. Cancer Treat. Rev. 41, 17-26.

Vonlaufen A., Phillips P.A., Xu Z., Goldstein D., Pirola R.C., Wilson J.S. and Apte M.V. (2008a). Pancreatic stellate cells and pancreatic cancer cells: An unholy alliance. Cancer Res. 68, 7707-7710.

Vonlaufen A., Joshi S., Qu C., Phillips P.A., Xu Z., Parker N.R., Toi C.S., Pirola R.C., Wilson J.S., Goldstein D. and Apte M.V. (2008b). Pancreatic stellate cells: Partners in crime with pancreatic cancer cells. Cancer Res. 68, 2085-2093.

Washington K., Berlin J., Branton P., Burgart L., Carter D. and Compton C. (2013). Protocol for the examination of specimens from patients with carcinoma of the exocrine pancreas. In. College of American Pathologists www.cap.org.

Yen T.W., Aardal N.P., Bronner M.P., Thorning D.R., Savard C.E., Lee S.P. and Bell R.H., Jr. (2002). Myofibroblasts are responsible for the desmoplastic reaction surrounding human pancreatic carcinomas. Surgery 131, 129-134.

Accepted January 21, 2020